Dynamic watermarks in images generated by diffusion models

Yunzhuo Chen[1], Jordan Vice[1], Naveed Akhtar[2,1], Nur Al Hasan Haldar[3,1], Ajmal Mian[1]

[1]The University of Western Australia, Perth, Australia

[2]The University of Melbourne, Melbourne, Australia

[3]Curtin University, Perth, Australia

`yunzhuo.chen@research.uwa.edu.au, naveed.akhtar1@unimelb.edu.au,`
`nur.haldar@curtin.edu.au, jordan.vice@uwa.edu.au, ajmal.mian@uwa.edu.au`

ABSTRACT

High-fidelity text-to-image diffusion models have revolutionized visual content generation, but their widespread use raises significant ethical concerns, including intellectual property protection and the misuse of synthetic media. To address these challenges, we propose a novel multi-stage watermarking framework for diffusion models, designed to establish copyright and trace generated images back to their source. Our multi-stage watermarking technique involves embedding: (i) a fixed watermark that is localized in the diffusion model's learned noise distribution and, (ii) a human-imperceptible, dynamic watermark in generates images, leveraging a fine-tuned decoder. By leveraging the Structural Similarity Index Measure (SSIM) and cosine similarity, we adapt the watermark's shape and color to the generated content while maintaining robustness. We demonstrate that our method enables reliable source verification through watermark classification, even when the dynamic watermark is adjusted for content-specific variations. Source model verification is enabled through watermark classification. o support further research, we generate a dataset of watermarked images and introduce a methodology to evaluate the statistical impact of watermarking on generated content.Additionally, we rigorously test our framework against various attack scenarios, demonstrating its robustness and minimal impact on image quality. Our work advances the field of AI-generated content security by providing a scalable solution for model ownership verification and misuse prevention.

1 INTRODUCTION

Driven by increasing demands, deep generative models have gained widespread attention in academic, industry and public domains. Recent advances have made photorealistic image generation more accessible (Bińkowski et al., 2018; Heusel et al., 2017; Salimans et al., 2016; Zhou et al., 2019) as exemplified by DALL·E 2 (Ramesh et al., 2022), Stable Diffusion (Rombach et al., 2022) and FLUX models (Labs, 2024). These models have also spurred the development of numerous image editing tools and text-to-video models including ControlNet (Zhang & Agrawala, 2023), Instruct-Pix2Pix (Brooks et al., 2022) and SORA (Brooks et al., 2024). While these models represent valuable digital assets, their widespread use raises critical ethical concerns, such as the potential for misuse in spreading false narratives, generating harmful representations, or infringing intellectual property (IP) rights.

To address these challenges, blind watermarking has emerged as a key strategy for IP protection and misuse prevention. Existing methods can be broadly categorized into two types: (1) embedding watermarks directly into the generative model to enable source verification (Wen et al., 2023; Fernandez et al., 2023; Peng et al., 2025; Min et al., 2024), and (2) embedding watermarks into generated images to protect content from unauthorized use (Zhao et al., 2023; Fernandez et al., 2023; Liu et al., 2023). However, different generation models and platforms may use varying content creation techniques. The diversity of generative models and platforms, each employing distinct algorithms, training processes, and representation formats, complicates the development of a universal watermarking solution. In addition, current watermarking methods face limitations. Moreover, fixed
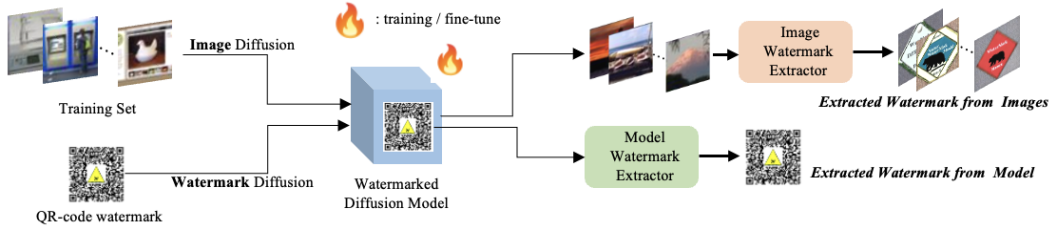
Figure 1: Overview of the proposed dual watermarking framework. The first stage embeds a fixed QR-code watermark directly into the diffusion model's latent space, ensuring model ownership verification. The second stage introduces a dynamic watermarking mechanism that imperceptibly modifies generated images, enhancing traceability while maintaining image quality.

watermarks embedded during training are often predictable and vulnerable to removal or tampering through reverse engineering or image-processing techniques (Moffat, 2019; Bińkowski et al., 2018; Heusel et al., 2017; Salimans et al., 2016; Zhou et al., 2019).

We propose an intuitive dual watermarking strategy, embedding: (*i*) a unique, model-specific QR code watermark directly into the diffusion model and, (*ii*) dynamic watermarks into images generated by the watermarked diffusion model. Our fixed QR-code watermark uniquely encodes model-specific metadata, within the diffusion model, including the IP address of machine it was trained on and date-time information. This ensures uniqueness, resistance to tampering, and complements dynamic watermarks in generated images for robust traceability through mutual verification. Our dynamic watermarking process that adjusts within feature and pixel spaces, thereby enhancing robustness through dynamic transformations based on the generated content. In the feature space, The high-level feature representations are extracted from the original and watermarked images using a pre-trained feature extractor. We calculate the cosine similarity (Rahutomo et al., 2012) between the features extracted from the images before and after applying watermark transformations. This step aims to enhance the separation of images by analyzing their feature similarities. In the pixel space, we evaluate the quality of images using the Structural Similarity Index (SSIM) (Channappayya et al., 2008), which quantifies the perceived differences between the original and transformed images. By mitigating the structural impact of the watermark embedding, we ensure that generated images are still properly classified post-watermarking.

Moreover, extensive research has shown that edges, frequency, and texture are the three key elements that influence human perception of subtle differences in images (Afchar et al., 2018; Chen et al., 2022; Cozzolino et al., 2017; Do & Vetterli, 2005; Chen et al., 2024). Leveraging this insight, we introduce a novel validation method to evaluate the impact of blind watermarking on image quality, utilizing 11 image statistics for assessment. The key contributions of this paper include:

- A dynamic watermarking strategy that enhances IP protection for generative models and enables traceability of generated content.

- An intuitive embedding methodology based on SSIM and cosine similarity, dynamically adjusting watermarks in feature and pixel spaces to improve robustness and minimize visual impact.

- A fixed QR-code watermark embedded within the diffusion model, cross-verifiable with dynamic watermarks in generated images, ensuring tamper resistance and content provenance.

- A novel blind watermark impact assessment mechanism that evaluates watermark visibility using 11 image statistics, addressing human-perceptible factors such as edges, frequency, and texture.

By addressing the limitations of existing methods and providing a robust, scalable solution, our work advances the field of AI-generated content security and contributes to ongoing efforts to mitigate ethical concerns in generative AI.
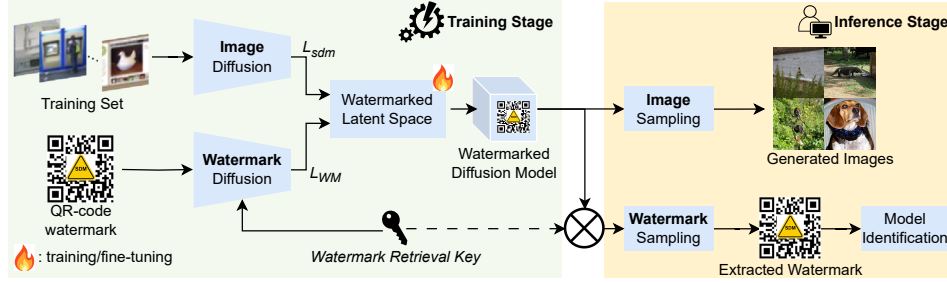
Figure 2: To verify model ownership, we embed a QR-code watermark into a target diffusion model, leveraging a watermark retrieval key to isolate watermark data and image data distributions. **(Left)** Through combined losses, the training stage contains both watermark and image diffusion stages to construct a common, watermarked latent space. **(Right)** Sampling from the watermarked model will generate images as usual. When provided with the watermark retrieval key as an input in the sampling process, the watermark will be extracted, allowing for model identification.

2 RELATED WORK

Fundamentally, diffusion models are generative frameworks built on the diffusion principles observed in non-equilibrium thermodynamics. Generally, these are implemented through a finite Markov chain (Geyer, 1992) for forward and reverse diffusion. Recently, diffusion models have been adapted for conditional image generation tasks, such as inpainting and text-guided generation and editing. Their iterative de-noising steps enables zero-shot image editing by guiding the generative process (Heusel et al., 2017; Salimans et al., 2016; Zhou et al., 2019).Watermarking techniques are actively researched to address copyright and misuse concerns in diffusion-based generative models. Here, we focus on the two main approaches, i.e, embedding watermarks within the model and, embedding watermarks in generated images.

Early research proposed methods for watermarking GANs by constructing mappings between trigger inputs and generator outputs with regularization constraints (Yu et al., 2021; Ong et al., 2021; Fei et al., 2022). However, these techniques cannot be directly applied to diffusion models due to architectural differences (Creswell et al., 2018; Cao et al., 2022). Additionally, Wen et al. proposed a robust tree-ring watermarking method against multiple image transformations and attacks (Wen et al., 2023). In addition, Li et al. introduced a diffusion-based watermarking approach, DiffWA (Li, 2023), which leverages the diffusion process to embed noise- and tamper-resistant watermarks.

In generative models, many works attempt to embed watermarks within the training dataset to protect the generative model's training data (Chai et al., 2020). However, this approach may be inefficient, as embedding new information requires costly retraining. Some research combines watermark embedding with the generative process (Gragnaniello et al., 2021; Wang et al., 2020), aligning more closely with model watermarking techniques. However, this approach faces two key limitations: (*i*) it applies primarily to GANs, while latent diffusion models (LDMs) are increasingly replacing GANs for most applications and, (ii) the watermark is embedded from the start of model training (Fei et al., 2022; Lin et al., 2022), a strategy that is challenging to sustain, given the resource-intensive nature of generative model training. Studies have shown that time-optimized fine-tuning of a generative model's latent decoder combined with an appropriate watermark extractor can achieve effective watermarking results (Fernandez et al., 2023).

3 PROPOSED METHOD

In this work, we propose two watermark embedding branches. (i) A *model* watermarking branch that embeds a fixed QR-code watermark into the learned noise distribution of the diffusion model, ensuring robust traceability and ownership verification. (ii) An *image* watermarking branch that embeds dynamic watermarks into generated images, balancing imperceptibility and resilience to attacks. Together, these branches enable model ownership verification and misuse prevention.

3.1 MODEL WATERMARKING

We employ the Stable Diffusion Model (SDM) (Rombach et al., 2022) for our experiments. To enable watermark embedding, we modify the latent diffusion process by introducing a modified Gaussian kernel. The data distribution is defined as $q(z)$, where z represents data in the latent space.

$$q(z_t|z_{t-1}) = N\left(z_t; \sqrt{\alpha_t}(z_{t-1} + \phi_t), \eta^2(1 - \alpha_t)I\right), \tag{1}$$

Here, α_t determines the step size for each diffusion step. ϕ_t is a constant schedule parameter in the diffusion process, which adjusts the input signal at each timestep t. The scheduling function can shift the input data, to assist in extracting and representing input features at specific timesteps. $\eta \in [0, 1]$ controls the noise scale and is a constant within the range $[0, 1]$.

The Watermark Diffusion process serves as an extension of the traditional SDM diffusion process, introducing a trigger *key*, which we denote as 'κ' (see Fig. 2) to alter the diffusion pathway for the variable z_t such that:

$$\hat{z}_t = \gamma_\kappa z_t + (1 - \gamma_\kappa)\kappa, \tag{2}$$

where γ_κ is a blending factor that modulates the influence of the watermark on the generated output. The reverse diffusion process retrieves the embedded watermark from the latent space for verification. The trigger key is integrated during sampling, as shown in Fig. 2.

Watermark Embedding can be accomplished by fine-tuning the host model ϵ_θ^o. In each iteration, we sample a data instance z_0 from the training dataset D_{train} and a watermark example z_0^w from the watermark dataset D_{wm}. Noise samples ϵ and ϵ_w are then drawn from $N(0, I)$ separately for task and watermark data, along with a timestep t sampled from Uniform($\{1, ..., T\}$).

For the sample z_0, the latent representation z_t at timestep t is computed using the latent diffusion process. For the watermark sample z_0^w, we first compute its latent representation z_t^w within the latent diffusion process, and then construct the state $\tilde{z}_t^w$ in the Watermark Diffusion Process based on z_t^w as follows:

$$\tilde{z}_t^w = \gamma_\kappa\left(\sqrt{\bar{\alpha}_t}z_0^w + \sqrt{1 - \bar{\alpha}_t}\epsilon_w\right) + (1 - \gamma_\kappa)\kappa. \tag{3}$$

The joint learning optimization objective for the latent and watermark diffusion processes, which also serves as the loss function for watermark embedding:

$$L_{WDP} = E_{t\sim[1,T],z_0,z_{w0},\epsilon_t}\left[\gamma_\epsilon\|\epsilon - \epsilon_\theta(z_t, t)\|^2 + \|\epsilon_w - \epsilon_\theta(\hat{z}_{wt}, t)\|^2\right], \tag{4}$$

Here, γ_ϵ is a weighting factor that balances the standard diffusion process ϵ and the watermark diffusion process ϵ_w during training.

Watermark Extraction to verify model ownership, can be achieved using the standard reverse diffusion process given the common latent space that was constructed through the combined diffusion processes discussed previously. The resulting output should be a reconstruction of the QR-code watermark that was used in the joint-training process. Given a model ϵ_θ, along with the known trigger κ and trigger factor γ_κ, we first sample z_T^w from $N(0, 1)$. Next, we calculate its corresponding state $\tilde{z}_t^w$ in the watermark diffusion process as follows:

$$\tilde{z}_t^w = \gamma_\kappa z_t^w + (1 - \gamma_\kappa)\kappa. \tag{5}$$

This state $\tilde{z}_t^w$ is then used as input to the model ϵ_θ to obtain the shared reverse noise to compute z_{t-1}^w. The extraction process follows the formula:

$$z_{t-1}^w = \frac{1}{\sqrt{\alpha_t}}\left[z_t^w - \frac{(1 - \alpha_t)}{\sqrt{1 - \bar{\alpha}_t}}\epsilon_\theta(\gamma_\kappa \hat{z}_t^w + (1 - \gamma_\kappa)\kappa, t)\right] + \sigma_t z, \tag{6}$$
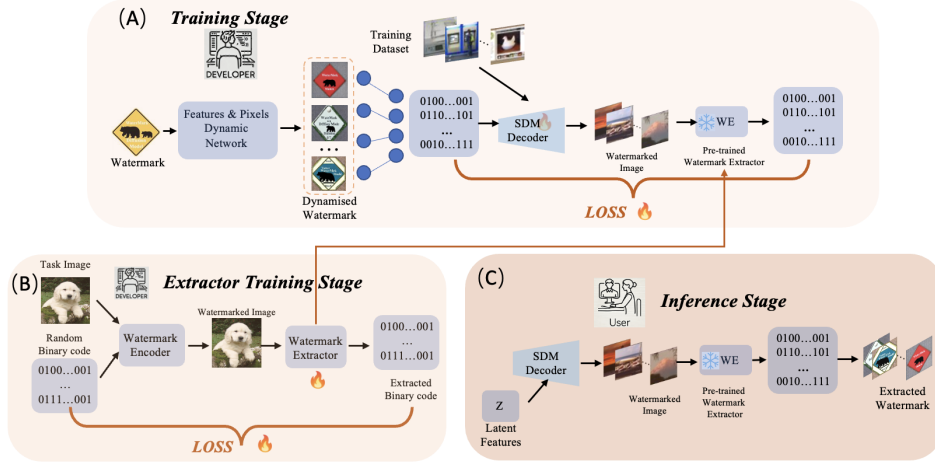
Figure 3: Overview of the dynamic watermarking framework, structured in three stages: (A) Training Stage: Fine-tunes the SDM decoder with a pre-trained watermark extractor to embed dynamic watermarks. (B) Extractor Training Stage: Trains the watermark extractor to encode and retrieve binary watermark information, maintaining reliability under transformations. (C) Inference Stage: Generates watermarked images using the SDM decoder, allowing the extractor to recover embedded watermarks for verification.

where σ_t is the noise level at timestep t and z is a random sample from $N(0, I)$. The selection of the trigger key and the factor γ_κ should ensure sufficient divergence between the state distribution in the Watermark Diffusion Process and that in the standard diffusion process.

3.2 IMAGE WATERMARKING

A dynamic watermarking mechanism embeds a unique watermark for each image. Watermarks vary in shape and colour while preserving key features of the reference watermark. In the feature space, we compute the cosine similarity between the original and transformed watermark images. Minimising this similarity enhances orthogonality, making extraction or tampering more difficult. In the pixel space, we maximise the SSIM to ensure high visual fidelity. These strategies enhance watermark robustness, imperceptibility, and classifiability without compromising the generative capabilities. The cosine similarity between the original f_o and transformed f_t watermark feature vectors is defined as:

$$\cos(\theta) = \frac{f_o \cdot f_t}{\|f_o\| \|f_t\|}. \tag{7}$$

By minimizing the cosine similarity, we aim to make f_o and f_t as orthogonal as possible within the high-dimensional feature space. This optimization ensures that the transformed watermark maintains its semantic structure while being imperceptible in the generated image.

In the pixel space, we calculate the SSIM between the original and transformed watermark images, denoted as I_o and I_t. The SSIM is defined as:

$$\text{SSIM}(I_o, I_t) = \frac{(2\mu_{I_o}\mu_{I_t} + C_1)(2\sigma_{I_o I_t} + C_2)}{(\mu_{I_o}^2 + \mu_{I_t}^2 + C_1)(\sigma_{I_o}^2 + \sigma_{I_t}^2 + C_2)}, \tag{8}$$

where μ_{I_o} and μ_{I_t} are the means of I_o and I_t, $\sigma_{I_o}^2$ and $\sigma_{I_t}^2$ are the variances, and $\sigma_{I_o I_t}$ is the covariance between I_o and I_t. Constants C_1 and C_2 are used for stability. By maximizing SSIM, we ensure that the transformed watermark image maintains high visual similarity to the original in the pixel space, thereby preserving visual quality.

To ensure that the watermark meets the requirements in both feature space and pixel space, we formulate an optimization problem, minimizing the following objective:

$$\min_{\text{transform parameters}} \left(\lambda_{cosine} \cdot \cos\theta - \lambda_{SSIM} \cdot \text{SSIM}(I_o, I_t) \right), \tag{9}$$

Where λ_{cosine} and λ_{SSIM} are weighting parameters that control the relative importance of cosine similarity and SSIM in the objective function. The goal is to reduce $\cos\theta$ between the original and transformed feature vectors, thereby increasing orthogonality. Concurrently, maximizing the SSIM between the original and transformed images in the pixel space preserves visual quality.

Image-to-binary sequences. In Fig. 3 (A), the watermark image is first converted into a binary sequence. We employ Huffman coding-based character encoding to reduce the size of binary sequence Gajjala et al. (2020). The average encoding length L_{avg} can be represented as: =

$$L_{\text{avg}} = \sum_{i=1}^{n} p_i l_i, \tag{10}$$

where p_i is the probability of character c_i, l_i is the encoding length for c_i, and n is the total number of characters in the set.

Image Watermark Embedding. Watermark embedding consists of two steps. First, we train a watermark extractor. Then, we fine-tune the SDM decoder to embed specific watermark information in all generated images.

As shown in Fig. 3(B), the watermark extractor W_E training builds on HiDDeN (Hsu & Wu, 1999). We embed binary watermark information by jointly optimizing the parameters of the watermark encoder and W_E. Ultimately, only W_E is retained as the watermark extractor. The watermark encoder takes a training image x_o and a binary watermark message m as inputs, producing a residual image x_δ. The watermarked image is obtained by scaling x_δ with a factor α. In each optimization step, a transformation T is randomly selected from a predefined set (e.g., cropping, compression) to generate the watermarked image. The extractor W_E then recovers the binary watermark m' as:

$$m' = W_E(T(x_o + \alpha x_\delta)) \tag{11}$$

The loss for the binary watermark information is calculated as:

$$L_E = -\sum_{i=1}^{k} [m_i \cdot \log \sigma(m_i') + (1 - m_i) \cdot \log(1 - \sigma(m_i'))] \tag{12}$$

In Fig. 3 Part (A), the SDM uses the latent vector z decoded by decoder to produce a generated image. To support multiple watermarks, the decoder D_m is extended to accept both the latent vector z and the condition vector e_i, which specifies which watermark to embed.

A training image is encoded by the SDM encoder E, and then combined with the embedding vector e_i (derived from the condition i) to control the watermark embedding as follows:

$$x_w' = D_m(E(x) \in R^{h \times w \times c}, e_i) \tag{13}$$

The pre-trained extractor network W_E recovers the watermark m_i' from the generated image x_w'. The binary watermark information loss ensures that the extracted watermark m_i' matches the target m_i specified by the condition i:

$$L_m = -\sum_{j=1}^{k} \left[m_i^{(j)} \cdot \log \sigma\left(m_i'^{(j)}\right) + \left(1 - m_i^{(j)}\right) \cdot \log\left(1 - \sigma\left(m_i'^{(j)}\right)\right) \right]$$

4   WATERMARK EXTRACTION RESULTS

To evaluate the effectiveness of our dual watermarking approach, we present the extracted watermarks from both branches: the *model* watermarking branch and the *image* watermarking branch.

4.1 MODEL WATERMARKING BRANCH

As shown in Fig. 4, our method effectively preserves the watermark's visibility and structure after extraction. The central logo undergoes minor deformation due to the diffusion process's inherent noise and transformations, which does not impact the QR code's scalability or embedded information.
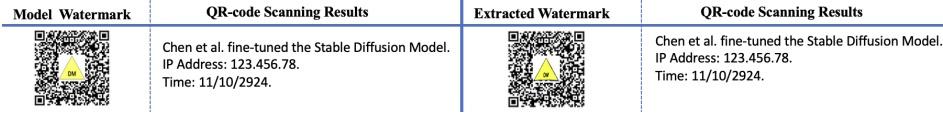

Figure 4: Extracted QR code watermark from the model watermark embedding branch. IP address and time are just hypothetical examples.

To evaluate the effectiveness of the extracted watermark, we analyze the Peak Signal-to-Noise Ratio (PSNR) (Korhonen & You, 2012) and SSIM between the original and extracted watermarks, comparing them with several mainstream models. Higher PSNR and SSIM values indicate better preservation of visual quality. As shown in Table 1, while our model does not achieve the highest PSNR and SSIM scores, it performs above average across these metrics, effectively balancing visual quality and watermark robustness.

Table 1: Comparison Based on PSNR and SSIM

Metric	DCT-DWT	SSL Watermark	FNNS	LDM	DiffEdit	HiDDeN	Ours
PSNR	39.5	31.1	32.1	34.0	31.2	32.0	35.67
SSIM	0.97	0.86	0.90	0.94	0.92	0.88	0.89

4.2 IMAGE WATERMARK EMBEDDING BRANCH

As shown in Figure 5, our custom-designed "Diffusion Model" and "Watermark" serve as the core information. Each extracted watermark retains this text, while dynamic transformations modify its appearance. These transformations enhance robustness and resilience, yet the classifier can still accurately verify the watermark's origin.

Figure 5: Extracted watermarks from the image watermark embedding branch. Each watermark has been dynamically transformed in shape and color.

4.3 IMPACT OF WATERMARK QUANTITY ON EXTRACTION ACCURACY

Our implementation supports up to six dynamic watermarks, maintaining robust extraction accuracy within this limit. To quantify this, we tested configurations with 2 to 6 watermarks. The extraction accuracy for each is reported in Table 2.

Table 2: Extraction Accuracy with Increasing Number of Watermarks

Number of Watermarks	2	3	4	5	6
Extraction Accuracy (%)	100.0	100.0	100.0	98.3	86.1

4.4 VALIDATION BASED ON STATISTICAL ANALYSIS

We use image statistics based on human perception as evaluation metrics. Based on the sensitivity coefficient s proposed by (Chen et al., 2024), we selected 11 image statistics measures with sensitivity values above 0.3, indicating a high sensitivity to changes in texture, edges, and frequency. Sensitivity ranges from 0 to 1, with higher values indicating greater sensitivity.

As shown in Table 3, the average change between watermarked and clean images across these metrics is approximately 5%. The GLCM Energy remains unchanged (0.00%), indicating that watermark embedding does not significantly affect image energy, which reflects texture uniformity and

Table 3: Image statistics comparison results. "Difference" refers to the percentage difference in data.Each Image statistics references:(Tsai et al., 2008),(De & Masilamani, 2013),(de Ridder, 1996),(Sebastian V et al., 2012),(Sebastian V et al., 2012),(Tahmid & Hossain, 2017),(He et al., 2005),(Frank et al., 2020),(Chan et al., 2018),(Freitas et al., 2018), (Chen et al., 2024)

	GLCM Contrast	GLCM Energy	Canny Edge	Variance Blur Measure	Mean spectrum	Edge Histogram	Entropy Strength	Sharpness Score	Saturation	Texture	Image Realism
Watermarked	354.80	0.19	46.41	1124.47	85.73	6.00	6.31	8836.29	63.04	5.92	1.55
Clean	371.23	0.19	48.34	1209.43	88.18	7.00	6.23	8903.23	67.00	5.65	1.42
Difference	4.63%	0.00%	4.16%	7.56%	2.86%	16.67%	1.27%	0.76%	6.28%	4.56%	8.39%

homogeneity. The Edge Histogram shows the largest difference (16.67%), highlighting its sensitivity to structural changes introduced by watermarking. This suggests that watermarking impacts edge distribution and frequency more than other visual characteristics, making the Edge Histogram an effective measure for detecting structural alterations.

4.5 WATERMARK ATTACK PERFORMANCE

We assessed the robustness of our watermarking method against common attacks, considering only those that preserve the visual quality of the generated image. For instance, while severe cropping (over 70%) reduces watermark recognition accuracy, it introduces visible tampering, making the attack perceptible. Thus, we focus on common attacks such as rotation, blurring, texture reduction, and image compression.

Table 4: Classification results of Watermarked Images under various attacks. The classification network distinguishes whether an image contains a watermark and then classifies the watermark.

	Attack Type						
	No Attack	Rotation	Blurring	Texture Reduction	Image Compression	Crop	Flip
Watermark Presence	100.00%	99.30%	100.00%	95.70%	98.50%	99.10%	100.00%
Watermark Classification	97.00%	95.98%	93.97%	93.94%	94.72%	94.05%	96.10%

As shown in Table 4, in the absence of attacks, "Watermark Presence" accuracy reached 100.00%, indicating perfect detection in undisturbed images. Texture reduction caused the largest drop (4.3%), likely due to its impact on watermark details, weakening detectability. Image compression, particularly lossy compression, also reduced accuracy to 98.50%. However, flip and crop attacks had minimal impact, maintaining accuracy at 100.00% and 99.10%, respectively.

For the "Watermark Classification" task, accuracy for unaltered images was high (97.00%). However, attacks slightly reduced classification accuracy. Blurring and texture reduction had the greatest impact, lowering accuracy to 93.97% and 93.94%, respectively, suggesting these attacks degrade visual features, making classification more challenging. Image compression and rotation also affected classification but to a lesser extent.

5 CONCLUSION

In this paper, we propose a dual approach for embedding fixed QR-codes within the diffusion process and dynamic watermarks in generated images. This integration enhances intellectual property protection and traceability in generated content. The dynamic watermark undergoes feature and pixel space transformations, increasing resistance to attacks while preserving image quality. It remains intact even under rotation, blurring, and compression. Statistical validation shows dual watermarking method has minimal impact on image quality, with only a 5% variation in key metrics such as edge and texture attributes, confirming the method's invisibility and robustness. Our work addresses critical challenges in the ethical use of AI-generated content, providing a scalable and effective mechanism for ownership verification and misuse prevention. Future research could explore extending this framework to other generative models and applications, further advancing the field of digital content security.

REFERENCES

Darius Afchar, Vincent Nozick, Junichi Yamagishi, and Isao Echizen. Mesonet: a compact facial video forgery detection network. In *2018 IEEE international workshop on information forensics and security (WIFS)*, pp. 1–7. IEEE, 2018.

Mikołaj Bińkowski, Danica J Sutherland, Michael Arbel, and Arthur Gretton. Demystifying mmd gans. *arXiv preprint arXiv:1801.01401*, 2018.

Tim Brooks, Aleksander Holynski, and Alexei A Efros. Instructpix2pix: Learning to follow image editing instructions. *arXiv preprint arXiv:2211.09800*, 2022.

Tim Brooks, Bill Peebles, Connor Holmes, Will DePue, Yufei Guo, Li Jing, David Schnurr, Joe Taylor, Troy Luhman, Eric Luhman, Clarence Ng, Ricky Wang, and Aditya Ramesh. Video generation models as world simulators. *OpenAI Technical Report*, 2024. URL https://openai.com/research/video-generation-models-as-world-simulators.

Hanqun Cao, Cheng Tan, Zhangyang Gao, Guangyong Chen, Pheng-Ann Heng, and Stan Z Li. A survey on generative diffusion model. *arXiv preprint arXiv:2209.02646*, 2022.

Lucy Chai, David Bau, Ser-Nam Lim, and Phillip Isola. What makes fake images detectable? understanding properties that generalize. In *European Conference on Computer Vision*, pp. 103–120. Springer, 2020.

Kelvin CK Chan, Raymond H Chan, and Mila Nikolova. A convex model for edge-histogram specification with applications to edge-preserving smoothing. *axioms*, 7(3):53, 2018.

Sumohana S Channappayya, Alan Conrad Bovik, and Robert W Heath. Rate bounds on ssim index of quantized images. *IEEE Transactions on Image Processing*, 17(9):1624–1639, 2008.

Yunzhuo Chen, Naveed Akhtar, Nur Al Hasan Haldar, and Ajmal Mian. Deepfake detection with spatio-temporal consistency and attention. In *2022 International Conference on Digital Image Computing: Techniques and Applications (DICTA)*, pp. 1–8. IEEE, 2022.

Yunzhuo Chen, Naveed Akhtar, Nur Al Hasan Haldar, Jordan Vice, and Ajmal Mian. A statistical image realism score for deepfake detection. In *2024 IEEE International Conference on Image Processing (ICIP)*, pp. 1391–1396. IEEE, 2024.

Davide Cozzolino, Giovanni Poggi, and Luisa Verdoliva. Recasting residual-based local descriptors as convolutional neural networks: an application to image forgery detection. In *Proceedings of the 5th ACM workshop on information hiding and multimedia security*, pp. 159–164, 2017.

Antonia Creswell, Tom White, Vincent Dumoulin, Kai Arulkumaran, Biswa Sengupta, and Anil A Bharath. Generative adversarial networks: An overview. *IEEE signal processing magazine*, 35 (1):53–65, 2018.

Kanjar De and V Masilamani. Image sharpness measure for blurred images in frequency domain. *Procedia Engineering*, 64:149–158, 2013.

Huib de Ridder. Naturalness and image quality: saturation and lightness variation in color images of natural scenes. *Journal of imaging science and technology*, 40(6):487–493, 1996.

Minh N Do and Martin Vetterli. The contourlet transform: an efficient directional multiresolution image representation. volume 14, pp. 2091–2106. IEEE, 2005.

Jianwei Fei, Zhihua Xia, Benedetta Tondi, and Mauro Barni. Supervised gan watermarking for intellectual property protection. In *IEEE International Workshop on Information Forensics and Security (WIFS)*, Shanghai, China, 2022.

Pierre Fernandez, Guillaume Couairon, Hervé Jégou, Matthijs Douze, and Teddy Furon. The stable signature: Rooting watermarks in latent diffusion models. In *Proceedings of the IEEE/CVF International Conference on Computer Vision*, pp. 22466–22477, 2023.

Joel Frank, Thorsten Eisenhofer, Lea Schönherr, Asja Fischer, Dorothea Kolossa, and Thorsten Holz. Leveraging frequency analysis for deep fake image recognition. In *International conference on machine learning*, pp. 3247–3258. PMLR, 2020.

Pedro Garcia Freitas, Luísa Peixoto Da Eira, Samuel Soares Santos, and Mylene Christine Queiroz de Farias. On the application lbp texture descriptors and its variants for no-reference image quality assessment. *Journal of Imaging*, 4(10), 2018.

Rishikesh R Gajjala, Shashwat Banchhor, Ahmed M Abdelmoniem, Aritra Dutta, Marco Canini, and Panos Kalnis. Huffman coding based encoding techniques for fast distributed deep learning. In *Proceedings of the 1st Workshop on Distributed Machine Learning*, pp. 21–27, 2020.

Charles J Geyer. Practical markov chain monte carlo. *Statistical science*, pp. 473–483, 1992.

Diego Gragnaniello, Davide Cozzolino, Francesco Marra, Giovanni Poggi, and Luisa Verdoliva. Are gan generated images easy to detect? a critical analysis of the state-of-the-art. In *2021 IEEE International Conference on Multimedia and Expo (ICME)*, pp. 1–6. IEEE, 2021.

Xiaofei He, Deng Cai, and Partha Niyogi. Laplacian score for feature selection. *Advances in neural information processing systems*, 18, 2005.

Martin Heusel, Hubert Ramsauer, Thomas Unterthiner, Bernhard Nessler, and Sepp Hochreiter. Gans trained by a two time-scale update rule converge to a local nash equilibrium. *Advances in neural information processing systems*, 30, 2017.

Chiou-Ting Hsu and Ja-Ling Wu. Hidden digital watermarks in images. *IEEE Transactions on image processing*, 8(1):58–68, 1999.

Jari Korhonen and Junyong You. Peak signal-to-noise ratio revisited: Is simple beautiful? In *2012 Fourth international workshop on quality of multimedia experience*, pp. 37–38. IEEE, 2012.

Black Forest Labs. Flux.1. `https://huggingface.co/black-forest-labs/FLUX.1-schnell`, 2024.

Xinyu Li. Diffwa: Diffusion models for watermark attack. In *2023 International Conference on Integrated Intelligence and Communication Systems (ICIICS)*, pp. 1–8. IEEE, 2023.

Dongdong Lin, Benedetta Tondi, Bin Li, and Mauro Barni. Cycleganwm: A cyclegan watermarking method for ownership verification. *arXiv preprint arXiv:2211.13737*, 2022.

Yugeng Liu, Zheng Li, Michael Backes, Yun Shen, and Yang Zhang. Watermarking diffusion model. *arXiv preprint arXiv:2305.12502*, 2023.

Rui Min, Sen Li, Hongyang Chen, and Minhao Cheng. A watermark-conditioned diffusion model for ip protection. *arXiv preprint arXiv:2403.10893*, 2024.

Alistair Moffat. Huffman coding. *ACM Computing Surveys (CSUR)*, 52(4):1–35, 2019.

Ding Sheng Ong, Chee Seng Chan, Kam Woh Ng, Lixin Fan, and Qiang Yang. Protecting intellectual property of generative adversarial networks from ambiguity attacks. In *Proceedings of the IEEE/CVF Conference on Computer Vision and Pattern Recognition (CVPR)*, pp. 3630–3639, Virtual, 2021. Computer Vision Foundation / IEEE.

Sen Peng, Yufei Chen, Cong Wang, and Xiaohua Jia. Intellectual property protection of diffusion models via the watermark diffusion process. In *International Conference on Web Information Systems Engineering*, pp. 290–305. Springer, 2025.

Faisal Rahutomo, Teruaki Kitasuka, Masayoshi Aritsugi, et al. Semantic cosine similarity. In *The 7th international student conference on advanced science and technology ICAST*, volume 4, pp. 1. University of Seoul South Korea, 2012.

Aditya Ramesh, Prafulla Dhariwal, Alex Nichol, Casey Chu, and Mark Chen. Hierarchical text-conditional image generation with clip latents. *arXiv preprint arXiv:2204.06125*, 1(2):3, 2022.

Robin Rombach, Andreas Blattmann, Dominik Lorenz, Patrick Esser, and Björn Ommer. High-resolution image synthesis with latent diffusion models. In *CVPR*, pp. 10684–10695, 2022.

Tim Salimans, Ian Goodfellow, Wojciech Zaremba, Vicki Cheung, Alec Radford, and Xi Chen. Improved techniques for training gans. *Advances in neural information processing systems*, 29, 2016.

Bino Sebastian V, A Unnikrishnan, and Kannan Balakrishnan. Gray level co-occurrence matrices: generalisation and some new features. *arXiv preprint arXiv:1205.4831*, 2012.

Taqi Tahmid and Eklas Hossain. Density based smart traffic control system using canny edge detection algorithm for congregating traffic information. In *2017 3rd International Conference on Electrical Information and Communication Technology (EICT)*, pp. 1–5. IEEE, 2017.

Du-Yih Tsai, Yongbum Lee, and Eri Matsuyama. Information entropy measure for evaluation of image quality. *Journal of digital imaging*, 21:338–347, 2008.

Sheng-Yu Wang, Oliver Wang, Richard Zhang, Andrew Owens, and Alexei A Efros. Cnn-generated images are surprisingly easy to spot... for now. In *Proceedings of the IEEE/CVF Conference on Computer Vision and Pattern Recognition (CVPR)*, pp. 8695–8704, 2020.

Yuxin Wen, John Kirchenbauer, Jonas Geiping, and Tom Goldstein. Tree-ring watermarks: Fingerprints for diffusion images that are invisible and robust. *arXiv preprint arXiv:2305.20030*, 2023.

Ning Yu, Vladislav Skripniuk, Sahar Abdelnabi, and Mario Fritz. Artificial fingerprinting for generative models: Rooting deepfake attribution in training data. In *Proceedings of the IEEE/CVF International Conference on Computer Vision (ICCV)*, pp. 14428–14437, Montreal, QC, Canada, 2021. IEEE.

Lvmin Zhang and Maneesh Agrawala. Adding conditional control to text-to-image diffusion models. *arXiv preprint arXiv:2302.05543*, 2023.

Yunqing Zhao, Tianyu Pang, Chao Du, Xiao Yang, Ngai-Man Cheung, and Min Lin. A recipe for watermarking diffusion models. *arXiv preprint arXiv:2303.10137*, 2023.

Sharon Zhou, Mitchell Gordon, Ranjay Krishna, Austin Narcomey, Durim Morina, and Michael S Bernstein. Hype: human-eye perceptual evaluation of generative models. 2019.